FAST AND ACCURATE SHADOW REGION IMAGING ALGORITHM USING RANGE DERIVATIVES OF DOUBLY SCATTERED SIGNALS FOR UWB RADARS

Shouhei Kidera and Tetsuo Kirimoto

Graduate School of Informatics and Engineering, University of Electro-Communications, Tokyo, Japan
Email: kidera@ee.uec.ac.jp

ABSTRACT

UWB (Ultra Wideband) radars have great promise for near field sensing systems, holding its high range resolution. It is particularly suitable for robotic or security sensors that must identify a target in optically blurry visions. Some recently developed radar imaging algorithms proactively employ multiple scattered components, which can enhance an imaging range compared to synthesizing a single scattered component. We have already proposed the SAR (Synthetic Aperture Radar) method considering a double scattered, which successfully expanded a reconstructible range of radar imagery with no preliminary knowledge of target or surroundings. However, this method requires an intensive computation and its spatial resolution is insufficient for clear boundary extraction such as edges or specular surfaces. As a substantial solution, this paper proposes a novel shadow region imaging algorithm based on a range derivative of double scattered signals. This new method accomplishes high-speed imaging, including a shadow region without any integration process, and enhances the accuracy with respect to clear boundary extraction. Some results from numerical simulations verify that the proposed method remarkably decreases the computation amount compared to that for the conventional method, enhancing the visible range of radar imagery.

1. INTRODUCTION

UWB pulse radar with high range resolution creates various applications for near field sensing. As such, a robotic sensor is one of the most promising applications, able to identify a human body even in optically blurry visibilities such as dark smog in disaster areas or high-density gas in resource exploration scenes. While various kinds of radar algorithms have been developed based on the aperture synthesis [1], the time reversal approach [2], or the GA-based solution for the domain integral equations [3], they are not suitable for the above applications because it is, generally, difficult to achieve both properties of low computation cost and high spatial resolution. As a high-speed and accurate imaging method feasible for complex-shaped targets, the RPM algorithm has been established [4]. This algorithm directly estimates an accurate DOA (Direction Of Arrival) with the global characteristic of observed range points, avoiding the difficulty of connecting them. The RPM is based on a simple idea, yet, it offers accurate and super-resolution surface extraction even for an extremely complicated boundary. However, they all have the unresolvable problem that aperture size strictly constrains the imaging range of target boundary. In many cases, the greater part of a target shape, such as a side of the target, falls into a shadow region that is never reconstructed since only single scattered components are used for imaging.

To resolve this difficulty and enhance imaging range, the SAR algorithm based on a double scattered path has been developed [5]. Although this method proves that the shadow region imaging is possible by positively using the double scattered signals without preliminary observations or target models, this method requires multiple integrations of the received signals, and incurs a large calculation cost. As a solution for these problems, this paper proposes a novel imaging algorithm based on the range derivative of doubly scattered signals, where an initial image obtained by RPM is used to the best effect. This method is based on an original relationship that each DOA of the double scattered points is strictly derived from the derivative of range points. This relationship enables us to directly estimate a target boundary corresponding to the doubly scattered centers without any integration procedures. The results of numerical simulations, investigating the two types of target shapes, show that this method accomplishes high-speed target boundary extraction, in situations which produce a shadow using the existing techniques.

2. SYSTEM MODEL

Fig. 1 shows the system model. It assumes the mono-static radar, and an omni-directional antenna is scanned along the x-axis. It is assumed that the target has an arbitrary shape with a clear boundary. The propagation speed of the radio wave c is assumed to be a known constant. A mono-cycle pulse is used as the transmitting current. The real space in which the target and antenna are located, is expressed by the parameters (x, z). The parameters are normalized by λ, which is the central wavelength of the pulse. $z > 0$ is assumed for simplicity. $s'(X, Z)$ is defined as the received electric field at the antenna

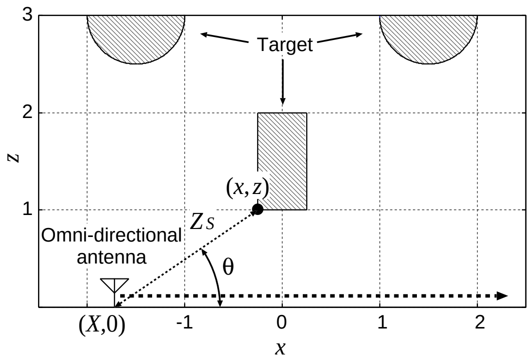

Fig. 1. System model in the 2-D model.

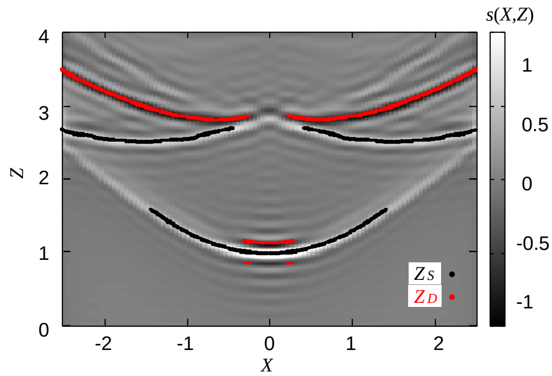

Fig. 2. Output of the Wiener filter for the multiple objects.

location $(x, z) = (X, 0)$, where $Z = ct/(2\lambda)$ is a function of time t. $s(X, Z)$ is defined as the output of the Wiener filter with the transmitted waveform. This procedure is detailed in [4].

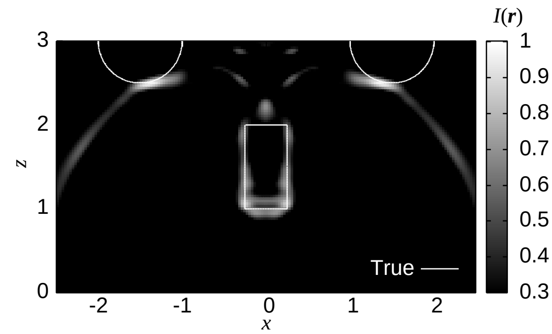

Fig. 3. Estimated image $I(\boldsymbol{r})$ with the conventional method.

3. CONVENTIONAL METHOD

As the conventional approach for enhancing the imaging range, the SAR employing the double scattered signal has been already developed [5]. In general, a double scattered wave propagates with a different path from that of a single scattered one. It therefore often provides independent information as to the two scattering points. This method calculates the image using double scattered waves as $I_2(\boldsymbol{r})$,

$$I_2(\boldsymbol{r}) = -\int_{\boldsymbol{r'}\in R}\int_{X\in\Gamma} I_1(\boldsymbol{r'})s\left(X, d_2(\boldsymbol{r},\boldsymbol{r'},X)/2\right)\mathrm{d}X\ \mathrm{d}\boldsymbol{r'}, \quad (1)$$

where $\boldsymbol{r'} = (x', z')$, R denotes the region of real space, and $d_2(\boldsymbol{r},\boldsymbol{r'},X) = \sqrt{(x-X)^2+z^2} + \sqrt{(x'-X)^2+z'^2} + \sqrt{(x-x')^2+(z-z')^2}$. $I_1(\boldsymbol{r})$ denotes the original SAR image. The minus sign in Eq. (1) creates a positive image focused by double scattered waves that have an antiphase relationship from a single scattered one. Eq. (1) expresses the aperture synthesis of the received signals by considering a double scattered path. The final image is defined as $I'(\boldsymbol{r}) = I_1(\boldsymbol{r})H(I_1(\boldsymbol{r}))/\{\max_{\boldsymbol{r}} I_1(\boldsymbol{r})\} + I_2(\boldsymbol{r})H(I_2(\boldsymbol{r}))/\{\max_{\boldsymbol{r}} I_2(\boldsymbol{r})\}$, where $H(*)$ is the Heaviside function.

The performance evaluation of this method is shown as follows. Fig. 2 shows the output of the Wiener filter, where the target boundary as in Fig. 1 is assumed. The received signals are calculated at 401 locations for $-2.5 \leq X \leq 2.5$. Fig. 3 shows the estimated image $I(\boldsymbol{r})$. This figure shows that the part of the side region of the rectangular target can be reproduced, and that the visible ranges of the circle and rectangular boundaries are remarkably expanded. The reason is that double scattered waves are effectively focused on the part of the target side using Eq. (1). It also claims that this method does not require target modeling or a priori information of the surroundings. However, it requires a triple integration for imaging and its calculation time goes up to around 60 sec for an Intel Pentium D 2.8 GHz processor.

4. PROPOSED METHOD

To overcome the problems described in the above, this paper proposes a high-speed imaging algorithm for the shadow region. This method employs target points preliminarily created by the RPM method, and directly reconstructs the target points corresponding to the double scattered signals, where each derivative of their range points is employed.

4.1. Principle of Proposed Method

First, a basic theory of the proposed method is described below. Here, two target points originating from doubly scattering are defined as $\boldsymbol{p}_1 = (x_1, z_1)$ and $\boldsymbol{p}_2 = (x_2, z_2)$, respectively. (X, Z_D) is defined as a range point of double scattered wave, which is extracted from the local minimum of $s(X, Z)$. $\boldsymbol{p}_L = (X, 0)$ denotes an antenna location. Then, the follow-

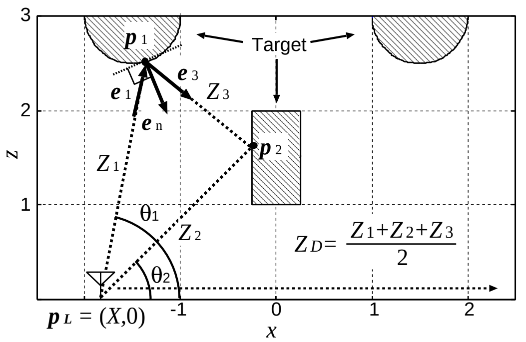

Fig. 4. Relationship among $\boldsymbol{p}_1$, $\boldsymbol{p}_2$ and $\boldsymbol{p}_L$.

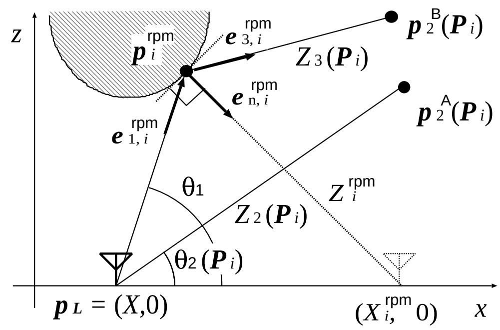

Fig. 5. Two candidates for $\boldsymbol{p}_2$ as $\boldsymbol{p}_2^A(\boldsymbol{P}_i)$ and $\boldsymbol{p}_2^B(\boldsymbol{P}_i)$.

ing equation holds,

$$\frac{\partial Z_D}{\partial X} = -\frac{\cos\theta_1 + \cos\theta_2}{2}, \tag{2}$$

where $\theta_1 = \cos^{-1}\left(\frac{x_1 - X}{Z_1}\right)$, $\theta_2 = \cos^{-1}\left(\frac{x_2 - X}{Z_2}\right)$, $Z_1 = \|\boldsymbol{p}_1 - \boldsymbol{p}_L\|$ and $Z_2 = \|\boldsymbol{p}_2 - \boldsymbol{p}_L\|$ are defined, and $0 \leq \theta_1, \theta_2 \leq \pi$ hold. According to this equation, once a first scattering point as $\boldsymbol{p}_1$ is determined, θ_2 is given as $\theta_2 = \cos^{-1}(-2\partial Z_D/\partial X - \cos\theta_1)$. Besides, if the normal vector $\boldsymbol{e}_\mathrm{n}$ on $\boldsymbol{p}_1$ is given, the law of reflection derives Z_2,

$$Z_2 = \frac{1}{2}\frac{Z_1^2 + (2Z_D - Z_1)^2 + 2(2Z_D - Z_1)(\boldsymbol{p}_1 - \boldsymbol{p}_L)\cdot\boldsymbol{e}_3}{(\boldsymbol{p}_1 - \boldsymbol{p}_L)\cdot\boldsymbol{e}_3 + 2Z_D - Z_1}, \tag{3}$$

where $\boldsymbol{e}_3 = \boldsymbol{e}_1 - 2(\boldsymbol{e}_\mathrm{n}\cdot\boldsymbol{e}_1)\boldsymbol{e}_\mathrm{n}$ holds with $\boldsymbol{e}_1 = (\boldsymbol{p}_1 - \boldsymbol{p}_L)/\|\boldsymbol{p}_1 - \boldsymbol{p}_L\|$. Furthermore, $\boldsymbol{p}_2$ obviously satisfies as $\boldsymbol{p}_2 = \boldsymbol{p}_1 + Z_3\boldsymbol{e}_3$, where $Z_3 = \|\boldsymbol{p}_2 - \boldsymbol{p}_1\|$ holds. Fig. 4 shows the relationship among the scattered points $\boldsymbol{p}_1$, $\boldsymbol{p}_2$ and the antenna location $\boldsymbol{p}_L$.

4.2. Incorporation with RPM method

Second, the proposed method makes uses of the preliminary estimated target points by RPM as the first scattering location $\boldsymbol{p}_1$ with its normal vector $\boldsymbol{e}_\mathrm{n}$. RPM basically converts the range points to the target points, satisfying an one-to-one correspondence. Here, we define each target and range point with the RPM as $\boldsymbol{p}_i^\mathrm{rpm} \equiv (x_i^\mathrm{rpm}, z_i^\mathrm{rpm})$ and $\boldsymbol{q}_i^\mathrm{rpm} \equiv (X_i^\mathrm{rpm}, Z_i^\mathrm{rpm})$, $(i = 1, \cdots N_\mathrm{T}^\mathrm{rpm})$, where $N_\mathrm{T}^\mathrm{rpm}$ is the total number of target points by RPM. In addition, each normal vector $\boldsymbol{e}_{\mathrm{n},i}^\mathrm{rpm}$ on $\boldsymbol{p}_i^\mathrm{rpm}$ is given as $\boldsymbol{e}_{\mathrm{n},i}^\mathrm{rpm} = \frac{(X_i^\mathrm{rpm} - x_i^\mathrm{rpm}, -z_i^\mathrm{rpm})}{Z_i^\mathrm{rpm}}$. This relationship is derived from the assumption that each antenna receives a strong echo from the target boundary, which is perpendicular to a direction for a line of sight [4].

This algorithm determines an optimal $\boldsymbol{p}_1$ from a set of the target points obtained by RPM, which is defined as $\mathcal{T}_\mathrm{rpm} = \left\{(x,z) \in \bigcup_{i=1}^{N_\mathrm{T}^\mathrm{rpm}} \boldsymbol{p}_i^\mathrm{rpm}\right\}$. Here, the parameter vector $\boldsymbol{P}_i$ is defined as $\boldsymbol{P}_i \equiv (\boldsymbol{R}_i^\mathrm{rpm}; \boldsymbol{Q}_D)$, where $\boldsymbol{Q}_D \equiv (\boldsymbol{p}_L, Z_D, \partial Z_D/\partial X)$ and $\boldsymbol{R}_i^\mathrm{rpm} \equiv (\boldsymbol{p}_i^\mathrm{rpm}, \boldsymbol{q}_i^\mathrm{rpm}, \boldsymbol{e}_{\mathrm{n},i}^\mathrm{rpm}, \boldsymbol{e}_{1,i}^\mathrm{rpm}, \boldsymbol{e}_{3,i}^\mathrm{rpm})$ hold. Here, $\boldsymbol{e}_{1,i}^\mathrm{rpm} = (\boldsymbol{p}_i^\mathrm{rpm} - \boldsymbol{p}_L)/\|\boldsymbol{p}_i^\mathrm{rpm} - \boldsymbol{p}_L\|$, and $\boldsymbol{e}_{3,i}^\mathrm{rpm}$ is determined with $\boldsymbol{P}_i$. Then, the proposed method determines the optimum candidate $\hat{\boldsymbol{p}_1}$ for each $\boldsymbol{Q}_D$ as

$$\hat{\boldsymbol{p}_1}(\boldsymbol{Q}_D) = \underset{\boldsymbol{p}_i^\mathrm{rpm}\in\mathcal{T}_\mathrm{RPM}}{\arg\min} \left\|\boldsymbol{p}_2^A(\boldsymbol{P}_i) - \boldsymbol{p}_2^B(\boldsymbol{P}_i)\right\|^2, \tag{4}$$

where, $\boldsymbol{p}_2^A(\boldsymbol{P}_i) \equiv \boldsymbol{p}_L + (Z_2(\boldsymbol{P}_i)\cos\theta_2(\boldsymbol{P}_i), Z_2(\boldsymbol{P}_i)\sin\theta_2(\boldsymbol{P}_i))$, and $\boldsymbol{p}_2^B(\boldsymbol{P}_i) \equiv \boldsymbol{p}_i^\mathrm{rpm} + Z_3(\boldsymbol{P}_i)\boldsymbol{e}_{3,i}^\mathrm{rpm}$ hold. Fig. 5 shows the relationship between two candidates for $\boldsymbol{p}_2$ as $\boldsymbol{p}_2^\mathrm{A}(\boldsymbol{P}_i)$ and $\boldsymbol{p}_2^\mathrm{B}(\boldsymbol{P}_i)$. The optimum second scattering point $\hat{\boldsymbol{p}_2}(\boldsymbol{Q}_D)$ is determined as $\hat{\boldsymbol{p}_2}(\boldsymbol{Q}_D) = \frac{\boldsymbol{p}_2^A(\hat{\boldsymbol{P}}) + \boldsymbol{p}_2^B(\hat{\boldsymbol{P}})}{2}$, where $\hat{\boldsymbol{P}}$ is defined as $\boldsymbol{P}_i$ when the evaluation value in the right term in Eq. (4) becomes minimum. Note that, this method does not employ any integration of the scattered signals and directly determines the doubly scattering points using the derivative of the range points.

5. PERFORMANCE EVALUATION IN NUMERICAL SIMULATION

This section presents numerical examples performed by RPM and the proposed method. Fig. 6 presents the estimated target points with the RPM and the proposed method, where (X, Z_S) and (X, Z_D) are extracted from $s(X, Z)$ as in Fig. 1. Also, $\partial Z_D/\partial X$ is calculated by difference approximation after smoothed with the Gaussian filter. This figure indicates that the proposed method accurately creates the target points around the side of the rectangular boundary. In addition, it has an great advantage in computation time, which required less than 0.4 sec for an Intel Pentium D 2.8 GHz processor. However, some fluctuations of the estimated points occur around the rectangular side, regardless of a noiseless situation. This is because this method employs the range derivative as $\partial Z_D/\partial X$, which tends to enhance small errors caused by the scattered waveform deformations or other interference

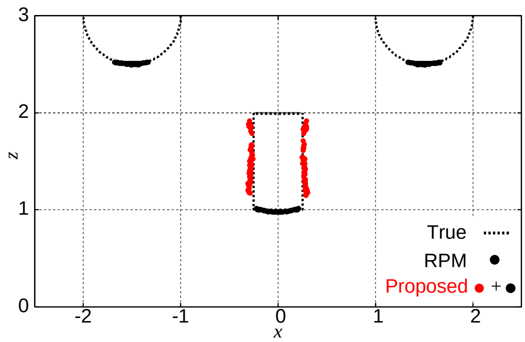

Fig. 6. Estimated image with the proposed method.

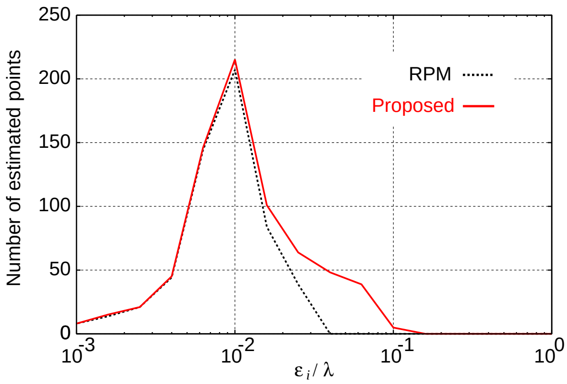

Fig. 7. Number of target points for each ϵ_i.

effects. Here, the quantitative analysis is introduced by ϵ_i defined as

$$\epsilon_i = \min_{\boldsymbol{p}_{\rm true}} \|\boldsymbol{p}_{\rm true} - \boldsymbol{p}_{\rm e}^i\|, \quad (i = 1, 2, ..., N_{\rm T}), \tag{5}$$

where $\boldsymbol{p}_{\rm true}$ and $\boldsymbol{p}_{\rm e}^i$ express the locations of the true and estimated target points, respectively. $N_{\rm T}$ is the total number of $\boldsymbol{p}_{\rm e}^i$. Fig. 7 plots the number of the estimated points for each value of ϵ_i. It verifies that the number of the accurate target points with the proposed method significantly increases around 0.03λ, simultaneously enhancing the imaging range.

Furthermore, the example in noisy situation is investigated, whereby white Gaussian noise is added to each received signal as $s'(X, Z)$. Fig. 8 shows the estimated points obtained by the proposed method, where the mean S/N is 30 dB. S/N is defined as the ratio of peak instantaneous signal power to the averaged noise power after applying the matched filter with the transmitted waveform. Although the accuracy of the estimated target points distorts due to the false range points extracted from noisy components, the whole image can offer a significant target boundary including the side of the rectangular boundary.

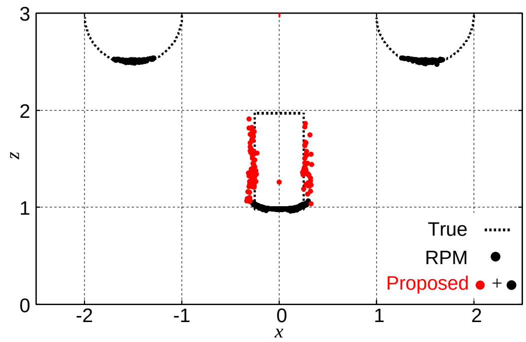

Fig. 8. Estimated image with the proposed method in S/N $= 30$ dB.

6. CONCLUSION

This paper proposed a novel imaging algorithm for expanding the imaging range, which efficiently utilizes the range derivative of the double scattered waves. This method has an outstanding advantage that it accomplishes an extremely high-speed imaging by specifying clear boundary extraction, simultaneously extending the visible region without any preliminarily knowledge of target or surroundings. In numerical simulation, the results proved that the proposed method substantially extended the imaging range with an remarkably high speed. It is more than 10^2 times improvement compared with that of the conventional SAR based method.

7. REFERENCES

[1] D. L. Mensa, G. Heidbreder and G. Wade, “Aperture Synthesis by Object Rotation in Coherent Imaging, *IEEE Trans. Nuclear Science.*, vol. 27, no. 2, pp. 989–998, Apr, 1980.

[2] D. Liu, J. Krolik, and L. Carin, “Electromagnetic Target Detection in Uncertain Media: Time-Reversal and Minimum-Variance Algorithms,” *IEEE Trans. Geosci. Remote Sens.*, vol.45, no.4, pp. 934–944, Apr, 2007.

[3] A. Massa, D. Franceschini, G. Franceschini, M. Pastorino, M. Raffetto and M. Donelli, “Parallel GA-based approach for microwave imaging applications,” *IEEE Trans. Antenna Propagat.*, vol. 53, no. 10, pp. 3118–3127, Oct, 2005.

[4] S. Kidera, T. Sakamoto and T. Sato, “Accurate UWB Radar 3-D Imaging Algorithm for Complex Boundary without Range Points Connections,” *IEEE Trans. Geosci. Remote Sens.*, vol. 48, no. 4, pp. 1993-2004, Apr., 2010.

[5] S. Kidera, T. Sakamoto and T. Sato, “Experimental Study of Shadow Region Imaging Algorithm with Multiple Scattered Waves for UWB Radars,” *Proc. of PIERS 2009*, Vol. 5, No. 4, pp. 393–396, Aug, 2009.